Eur. Phys. J. D **22**, 319–331 (2003)
DOI: 10.1140/epjd/e2003-00020-2

THE EUROPEAN PHYSICAL JOURNAL D

Coherent and incoherent phonon processes in artificial atoms

L. Jacak[1], P. Machnikowski[1,a], J. Krasnyj[2,b], and P. Zoller[3]

[1] Institute of Physics, Wrocław University of Technology, Wybrzeże Wyspiańskiego 27, 50–370 Wrocław, Poland
[2] Institute of Mathematics, University of Opole, Oleska 48, 45–051 Opole, Poland
[3] Institut für Theoretische Physik, Universität Innsbruck, Technikerstrasse 25, 6020 Innsbruck, Austria

Received 30 August 2002 / Received in final form 25 November 2002
Published online 28 January 2003 –

Abstract. Carrier–phonon interaction in semiconductor quantum dots leads to three classes of phenomena: coherent effects (spectrum reconstruction) due to the nearly-dispersionless LO phonons, incoherent effects (transitions) induced by acoustical phonons and dressing phenomena, related to non-adiabatic, sub-picosecond excitation. Polaron spectra, relaxation times and dressing-related decoherence rates are calculated, in accordance with experiment.

PACS. 68.65.Hb Quantum dots – 63.20.Kr Phonon-electron and phonon-phonon interactions – 03.65.Yz Decoherence; open systems; quantum statistical methods

1 Introduction

The properties of natural atoms have been studied for decades and are well-known now. There is no principal obstacle that would prevent one from isolating a single atom or a group of atoms (or ions) and reducing their uncontrolled interaction with environment to any degree. The resulting isolated system may be then manipulated with great precision *e.g.* by laser light. In recent years, the feasibility of this scenario was confirmed experimentally by trapping single ions and linear chains of ions, coupling them in a controlled way to the oscillatory "phonon" mode of the chain and coherently manipulating this system by laser light (for a review, see [1]). In this way the implementation of the quantum logical operations is possible [2–5].

A man-made analogue of these atomic systems are quasi zero-dimensional semiconductor structures, called quantum dots (QDs) [6]. They may be obtained in different ways, one of which is spontaneous aggregation of a semiconductor compound which has been epitaxially grown on a different compound (*e.g.* InAs on GaAs). Due to the strain generated by the lattice constant mismatch, after growing a few atomic layers of InAs the system undergoes the Stransky-Krastanov transition and the uniform layer is transformed into a random distribution of aggregates (self-assembled QDs), whose radius is of several tens of nanometers and height may be as low as 2 nm, lying on a very thin wetting layer of InAs. This is then capped again with the GaAs (or inserted in a more complicated structure suitable for experimental purpose).

A carrier localized in a quantum dot has a discrete spectrum resulting from the effective confinement potential induced by the band discontinuity between the InAs island and the surrounding GaAs bulk, strongly modified by crystal stress [7]. Since the self-assembled InAs/GaAs dots are usually lens-shaped, the confinement is much stronger in the growth direction than in the perpendicular plane. The characteristic energies for the in-plane excitations of electrons are of order of tens of meV. The excited levels are nearly degenerated, leading to the formation of shells in the spectrum [8]. Above the discrete spectrum there is the 2D continuum of wetting layer states and then the 3D continuum of the GaAs bulk. Because of the similarity of the QD spectra to the atomic ones these quasi-0D semiconductor systems were called artificial atoms [9,10]. Coherent phenomena occurring in these systems [11–14] open the possibility for their application in quantum information processing using either spin degrees of freedom [15] or orbital ones [16], or both [17].

There are a few advantages of the artificial quantum dots over the natural atoms: Their properties are governed by growth conditions and therefore are relatively flexible. The stress distribution favors the creation of chains of coupled dots when one layer is grown over another. The small inter-level spacing increases the magnetic field effects, thus supplying another degree of freedom for modifying the system properties. Using optical excitation and doping techniques it is possible to populate the dots with a definite number of carriers, creating charged and neutral (excitonic) states. Controlled entanglement in such "artificial molecules" has been demonstrated [18]. The industry-scale semiconductor technology is well developed, raising hopes for easy integration of the future QD nano-devices

[a] e-mail: machnik@if.pwr.wroc.pl
[b] On leave from Odessa University, Ukraine.

with the existing microelectronics. Finally, the technology of isolating a single dot for investigation [19] and coherent control [20] seems to be more accessible than the ion trapping techniques.

On the other hand, quantum dots have much more complicated properties, resulting from anisotropy [21], inhomogeneous composition [22], crystal stress [7,23], possibly irregular shape and presence of many types of carriers (electrons and three hole branches for GaAs-type semiconductors). Moreover, they are not isolated systems. They are embedded in the macroscopic crystal and interacting with other carriers, crystal defects and lattice excitations. While the former two kinds of interaction may be eliminated by optimizing the manufacturing conditions, lowering temperature and decreasing the excitation power, the lattermost is unavoidable.

There are three major mechanisms of carrier-phonon interaction [24]:

(1) Coulomb interaction with the lattice polarization induced by the relative shift of the positive and negative sub-lattices of the polar compound, described upon quantization by longitudinal optical (LO) phonons;
(2) deformation potential coupling describing the band shifts due to lattice compression, *i.e.* longitudinal acoustical (LA) phonons;
(3) Coulomb interaction with piezoelectric field generated by shear crystal deformation (transversal acoustical, TA, phonons).

The lattermost effect is weak in InAs/GaAs systems but may be of more importance for the properties *e.g.* of GaN dots [25–27].

One may expect that the carrier-phonon interaction should lead to transitions between carrier states. It was predicted theoretically [28,29] that phonon-induced relaxation from excited states should be slow due to the bottleneck effect: the trapped carrier wavefunction is localized on approximately 10 lattice constants and high energy acoustic phonons do not effectively couple to carriers due to the wavelength mismatch, while optical phonons have very weak dispersion around $\mathbf{k} = \mathbf{0}$ so that energy conservation would require a strictly defined energy distance between the carrier levels. Experiments on large ensembles of dots show, however, that the carriers relax from the excited states in a few tens of picoseconds by emitting one [30] or more [31] LO phonons. The cascade relaxation rate is limited by the final step, from the lowest excited to the ground state. The observed LO phonon relaxation, apparently contrary to the bottleneck idea, can be explained by the fact that in the large ensemble of inhomogeneously sized dots some of them satisfy the energy conservation [31].

Another manifestation of the carrier-phonon interaction in confined semiconductor systems are the phonon replicas in the emission and absorption spectra, corresponding to simultaneous photon and phonon absorption or emission. Such phonon-assisted peaks may be found both in ensemble [32,33] and single-dot [34] experiments. These peaks are much stronger than could be expected on the grounds of the adiabatic theory: the overlap of the electron and hole wavefunction in the ground state of the charge-neutral exciton should lead to the cancellation of the polar interaction between the exciton and the LO phonon [35]. It was shown [36] that non-adiabatic effects, *i.e.* carrier transitions between ground and excited states induced by the lattice dynamics lead to the increase of the phonon-assisted peak strength in accordance with experiment.

Apart from these incoherent phonon processes, carrier-phonon interaction induces also coherent effects. The far infrared (FIR) magnetospectroscopy of quantum dots shows distinct anti-crossings of electron [21,37] or exciton [38] levels each time they are separated by a multiple of the LO phonon energy. Such anti-crossings are an evidence of the presence of polaron states, *i.e.* coherent superpositions of carrier and phonon states. The appearance of such coherent effects is possible because of the quasi-dispersionless character of the strongly coupled LO phonons [39], assuring LO phonon-induced dephasing times much longer than any other relevant process.

Thus, there are two incompatible concepts: according to the coherent polaron idea, the carrier–LO phonon interaction leads to the reconstruction of the spectrum and to the formation of hybrid states. In this picture, the interaction with phonons induces coherent oscillations between the excited state and the ground state accompanied by a phonon [21,39]. On the contrary, the LO phonon-induced relaxation [30,31] assumes a non-invertible transition from the excited state to the ground state, after which the final state dissolves in the phonon continuum. In this paper we re-examine this issue theoretically by introducing the system description in the basis of polaron states including, by definition, the coherent LO phonon effects. As the carrier–LO phonon Hamiltonian is diagonal in the new basis, there is no channel for the purely LO phonon relaxation processes, which is consistent with the coherent polaron picture found in the FIR experiments. However, two-phonon processes including acoustical phonons (which makes them incoherent by providing a broad, weakly coupled continuum) take place on the timescale of tens of picoseconds, in agreement with the relaxation experiments [30,31].

Introducing the canonical transformation to the polaronic basis, we reproduce the earlier numerical results [21] in the analytical form. This approach not only facilitates the interpretation of the results but also is a good starting point for the quantitative description of the relaxation phenomena. It leads to a uniform approach to both LO–LA and LO–TA phonon processes, generalizing the bottleneck mechanism [29] to the two-phonon case and explaining the different nature of the anharmonicity-induced relaxation (no bottleneck). Another advantage is the feasibility of taking more exciton levels into account while discussing the excitonic polaron spectrum (as compared to the numerical study [38]) and describing the "shell effects" in the exciton-phonon resonances.

We address also another phenomenon related to the phonon-induced coherence loss. The recent time-resolved single-dot experiment [19] showed a partial decay of the

initial signal coherence on a picosecond scale. The coherence loss was then stopped at a relatively high, temperature dependent level, with a subsequent exponential decay limited by the exciton lifetime (~ 1 ns) at low temperatures. Such a behavior of the system polarization after an infinitely short exciting pulse was theoretically accounted for in the single-state (independent boson) model within the linear response regime [35] and then generalized to higher orders and to sequences of pulses [40]. We show that this partial coherence loss is a manifestation of a general dressing phenomenon, where the lattice reaction and formation of the coherent phonon cloud is a slow process following a fast (non-adiabatic) carrier excitation. Unlike the earlier model [35], the present description sacrifices exact solvability in order to include higher excitonic states (non-adiabatic effects).

It should be stressed that the presented model, although reasonable for the description of the essential effects, does not account for the full complexity of the quantum dot structure and the related phonon modes. Real dots have irregular shape, inhomogeneous composition [22] and complicated strain distribution [7,23]. Moreover, apart from the bulk GaAs phonon modes, other modes may appear, *e.g.* surface ones [41]. Another limitation of the presented approach is related to neglecting multiple-phonon processes (except for the essential LO–LA and LO–TA ones). This restricts the applicability of the results to relatively low temperatures (approximately below 100 K for GaAs material parameters). A more exact description should include *e.g.* the elastic phonon processes (exciton-phonon collisions) which also contribute to exciton decoherence [42].

The paper is organized as follows. Section 2 introduces the model of the system to be discussed. In Section 3 we analyze the polaron spectra for an electron and an exciton in a InAs/GaAs quantum dot. Section 4 contains the discussion of the relaxation rates. The phonon dressing issue is addressed in Section 5. The final Section 6 contains the conclusions.

2 The model

We will consider the system consisting of a single carrier or one interacting electron-hole pair localized in a dot, described in the effective mass approximation. The system is placed in a magnetic field oriented in the growth direction. We will assume that the confinement potential is harmonic, isotropic or weakly anisotropic in the dot plane (xy) and much stronger in the growth direction (z). In spite of the complicated dot structure the simple harmonic approximation proves to be very accurate [43]. Thus, the single carrier Hamiltonian for the electron ($i = \mathrm{e}$) or hole ($i = \mathrm{h}$) may be written in the coordinate representation

$$H_i = -\frac{\hbar^2}{2m_i}\nabla_i^2 + \frac{1}{2}m_i\omega_i^2 r_{i\perp}^2 + \frac{\hbar\omega_{\mathrm{c},i}}{2}\left(-\mathrm{i}\frac{\partial}{\partial\varphi_i}\right) + U^{(i)}(z_i) + W^{(i)}(\mathbf{r}_{i\perp}), \quad (1)$$

where $\mathbf{r}_{i\perp} = r_i(\cos\varphi_i, \sin\varphi_i)$ is the projection of the electron/hole position on the xy plane, $\omega_i^2 = \omega_{0,i}^2 + \omega_{\mathrm{c},i}^2/4$, $\omega_{\mathrm{c},i} = eB/m_i$ (cyclotron frequency) and $U^{(i)}(z_i) = \frac{1}{2}m_i\omega_{z,i}^2 z_i^2$, $\omega_{z,i} \gg \omega_{0,i}$. The last term in (1) describes the weak anisotropy of the confining potential,

$$W^{(i)}(\mathbf{r}_{i\perp}) = \frac{\lambda}{2}m_i\omega_{0,i}^2 r_{i\perp}^2 \cos 2\varphi_i. \quad (2)$$

The Coulomb interaction between the carriers is described by

$$H_{\mathrm{C}} = -\frac{e^2}{4\pi\epsilon_0\epsilon_{\mathrm{s}}}\frac{1}{|r_{\mathrm{e}} - r_{\mathrm{h}}|}\,. \quad (3)$$

Three branches of phonons, LO, LA and TA, will be included with the Hamiltonian given by

$$H_{\mathrm{ph}} = \sum_{s,\mathbf{k}} \hbar\omega_s(\mathbf{k}) b_{s,\mathbf{k}}^\dagger b_{s,\mathbf{k}}, \quad (4)$$

where s denotes the phonon branch ($s = \mathrm{o}$ for LO, $s = \mathrm{l}$ for LA and $s = \mathrm{t}$ for TA) and $\omega_s(\mathbf{k})$ are the corresponding frequencies. The electrons and holes interact with the LO phonons by the polar coupling, described by the Fröhlich Hamiltonian

$$H_F^{(i)} = \mp\frac{1}{\sqrt{N}}\sum_{\mathbf{k}}\frac{e}{k}\sqrt{\frac{\hbar\omega_{\mathrm{o}}(\mathbf{k})}{2v\epsilon_0\tilde{\epsilon}}}\left(b_{\mathrm{o},\mathbf{k}} + b_{\mathrm{o},-\mathbf{k}}^\dagger\right)\mathrm{e}^{\mathrm{i}\mathbf{k}\cdot\mathbf{r}_i}, \quad (5)$$

where $i = \mathrm{e}, \mathrm{h}$, v is the volume of the crystal cell and $\tilde{\epsilon} = (1/\epsilon_\infty - 1/\epsilon_{\mathrm{s}})^{-1}$ is the effective dielectric constant ("$-$" for electrons, "$+$" for holes).

Both types of carriers interact also with the LA phonons *via* the deformation potential coupling, as described by the Hamiltonian

$$H_{\mathrm{DP}}^{(i)} = \frac{1}{\sqrt{N}}\sum_{\mathbf{k}}\sigma_i\sqrt{\frac{\hbar k}{2\varrho v c_{\mathrm{l}}}}\left(b_{\mathrm{l},\mathbf{q}} + b_{\mathrm{l},-\mathbf{q}}^\dagger\right)\mathrm{e}^{\mathrm{i}\mathbf{k}\cdot\mathbf{r}_i},\ i = \mathrm{e}, \mathrm{h}, \quad (6)$$

where σ_i is the deformation potential constant for electrons or holes, ϱ is the crystal density, c_{l} is the speed of longitudinal sound.

In addition, the anharmonic mechanism for the LO phonon decay into a TA phonon and another LO phonon (the most important channel in GaAs bulk [44,45]) will be included,

$$H_{\mathrm{anh}} = \sum_{\mathbf{q},\mathbf{k}} W(\mathbf{k},\mathbf{q}) b_{\mathrm{o},\mathbf{k}}^\dagger b_{\mathrm{o},\mathbf{k}-\mathbf{q}}\left(b_{\mathrm{t},\mathbf{q}} + b_{\mathrm{t},-\mathbf{q}}^\dagger\right) + \mathrm{h.c.} \quad (7)$$

3 Coherent LO phonon effects

In this section we study the spectrum of the system composed of the confined carriers and the LO phonons. The LO phonon spectrum is characterized by a gap which is comparable to the carrier excitation energy and by a

Table 1. The GaAs material parameters used in the calculations (after [7,46,47]).

Electron mass	m_e	$0.067m_0$
Hole mass	m_h	$0.62m_0$
Static dielectric constant	ϵ_s	13.2
High-frequency dielectric constant	ϵ_∞	10.9
Optical phonon energy at $\mathbf{k}=\mathbf{0}$	$\hbar\Omega_0$	36 meV
Longitudinal sound speed	c_l	5150 m/s
Transversal sound speed	c_t	2850 m/s
Deformation potential for electrons	σ_e	6 eV
Density	ϱ	5360 kg/m^3

very weak dispersion. Therefore, the carrier–LO phonon interaction is always in the strong coupling regime, which results in coherent carrier-phonon dynamics, instead of phonon-induced incoherent transitions [21,39]. Hence, if sufficiently short timescales are involved, the incoherent effects induced by the LO phonon dispersion (characterized by 100 ps timescale, see Sect. 5) may be neglected. In our description we assume dispersionless LO phonons, $\omega_\mathrm{o}(\mathbf{k})=\Omega$. It may be shown that in the case of sufficiently strongly coupled LO phonon band of narrow but finite width the spectrum has the same properties [37,39].

We will refer our quantitative results to an InAs/GaAs self-assembled quantum dot. The electron and hole effective masses for the stretched InAs become close to the GaAs values [7]. We assume $m_\mathrm{e}=0.067m_0$, $m_\mathrm{h}=0.62m_0$ [46]. The single-carrier excitation energies $\hbar\omega_{0,i}$ depend on the detailed microscopic dot structure which is usually not exactly known. We assume that at zero magnetic field the noninteracting electron and hole wavefunctions should be the same, hence $\omega_{0,\mathrm{h}}/\omega_{0,\mathrm{e}}=m_\mathrm{e}/m_\mathrm{h}$. This is not necessarily the case since the potential walls at the dot boundary are not infinite and the carries are influenced by nonuniform composition and stress in different ways. Nevertheless, without any additional knowledge on the dot stoichiometry and stress distribution this seems a reasonable choice. The other material parameters are collected in Table 1.

Since the confinement in the z-direction is very strong, we will assume that the carriers are always in the ground state with respect to the dynamics in this direction.

3.1 Single carrier polaron states

Let us start with the simplest case of a single electron in the dot. The eigenstates of the Hamiltonian H_e (Eq. (1)) in the isotropic limit (*i.e.* neglecting $W(\mathbf{r}_\perp)$) are the Fock-Darwin states (for a review, see *e.g.* [6]). The dot anisotropy (described by Eq. (2)) may be included perturbatively.

The electron–LO phonon Hamiltonian, expressed in the occupation number representation in the basis of the eigenstates of (1) reads

$$\begin{aligned} H_{\mathrm{e-LO}} &= H_\mathrm{e}+H_\mathrm{LO}+H_\mathrm{F}^{(\mathrm{e})} \\ &= \sum_n \epsilon_n a_n^\dagger a_n + \hbar\Omega\sum_{\mathbf{k}} b_{\mathrm{o},\mathbf{k}}^\dagger b_{\mathrm{o},\mathbf{k}} \\ &\quad + \frac{1}{\sqrt{N}}\sum_{n,n',\mathbf{k}} F_{nn'}^{\mathrm{e-LO}}(\mathbf{k}) a_n^\dagger a_{n'}\left(b_{\mathrm{o},\mathbf{k}}+b_{\mathrm{o},-\mathbf{k}}^\dagger\right), \end{aligned} \tag{8}$$

with the electron–LO phonon interaction functions:

$$F_{nn'}^{\mathrm{e-LO}} = \frac{e}{k}\sqrt{\frac{\hbar\Omega}{2v\epsilon_0\tilde{\epsilon}}}\mathcal{F}_{nn'}(\mathbf{k}), \tag{9}$$

where the form-factors are

$$\mathcal{F}_{nn'}(\mathbf{k}) = \int \mathrm{d}^3 r \Psi_n^*(\mathbf{r})\exp\left(\mathrm{i}\mathbf{k}\cdot\mathbf{r}\right)\Psi_{n'}(\mathbf{r}) \tag{10}$$

$$= g_{nn'}(k_\perp,\varphi_0)\mathrm{e}^{-\left(\frac{k_\perp l_\mathrm{B}}{2}\right)^2}\mathrm{e}^{-\left(\frac{k_z l_z}{2}\right)^2}, \tag{11}$$

where $l_\mathrm{B}=\sqrt{\hbar/(m_\mathrm{e}\omega_\mathrm{e})}$ and $l_z=\sqrt{\hbar/(m_\mathrm{e}\omega_{z,\mathrm{e}})}$ are the confinement lengths in lateral (xy) and z-direction and $g_{nn'}$ are certain functions (polynomial in $k_\perp$ [48]). The essential feature of the coupling functions are the exponents responsible for the bottleneck effect, limiting effectively the carrier–phonon interaction to the phonons with wavelengths not much shorter than the dot size.

The spectrum of the polaron may be found using the canonical transformation introduced by Davydov and Pestryakov [49]. The details of the diagonalization procedure for confined states are given elsewhere [48,50]. The main idea is to write the Hamiltonian in terms of polaron operators, defined as

$$\alpha_\nu = \mathrm{e}^{\mathsf{S}} a_\nu \mathrm{e}^{-\mathsf{S}},\ \beta_{\mathrm{o},\mathbf{k}} = \mathrm{e}^{\mathsf{S}} b_{\mathrm{o},\mathbf{k}} \mathrm{e}^{-\mathsf{S}},$$

with the anti-hermitian operator

$$\mathsf{S} = \sum_{n,n',\mathbf{k}} \frac{F^{\mathrm{e-LO}}(\mathbf{k})}{E_{n'}-E_n+\hbar\Omega} a_n^\dagger a_{n'}(b_{\mathrm{o},\mathbf{k}}-b_{\mathrm{o},-\mathbf{k}}^\dagger). \tag{12}$$

The polaron energies E_n are found from the equation

$$E_n = \epsilon_n - \sum_{n'}\frac{J_{nn'}}{E_{n'}-E_n+\hbar\Omega}, \tag{13}$$

where

$$J_{nn'} = \frac{1}{N}\sum_{\mathbf{k}} |F_{nn'}^{\mathrm{e-LO}}(\mathbf{k})|^2.$$

Neglecting residual multi-polaron and multi-phonon interaction terms [49], the Hamiltonian (8) attains a diagonal form,

$$H_{\mathrm{e-LO}} = \sum_n E_n \alpha_n^\dagger \alpha_n + \hbar\Omega\sum_{\mathbf{k}} \beta_{\mathrm{o},\mathbf{k}}^\dagger \beta_{\mathrm{o},\mathbf{k}}. \tag{14}$$

The solution of the equation (13), restricted to the three lowest states, is presented in the Figure 1 and compared to

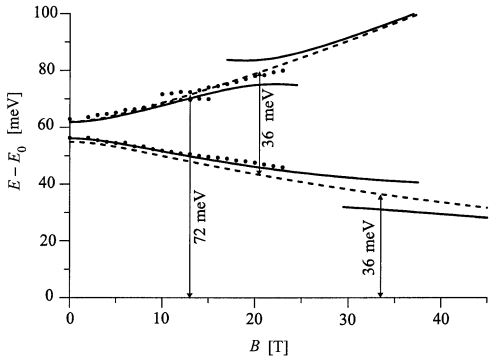

Fig. 1. Polaron spectrum for a weakly elliptical quantum dot in the presence of magnetic field for the dot parameters fitted to the experimental data of reference [21]: $\hbar\omega_{0,\mathrm{e}} = 57.8$ meV, $\lambda = 0.122$. The polaron levels (solid lines) are compared to the levels obtained without non-diagonal (non-adiabatic) Fröhlich coupling (dashed lines) and to the experimental data (dots).

the experimental data [21]. The most interesting features on this plot are level anti-crossings which appear when a ground level plus one or more LO phonon energy is degenerate with an excited level. The Fröhlich interaction lifts this degeneracy leading to the anti-crossing effect. The analytical method presented above accounts for the one-phonon resonances, while the two-phonon resonance is a higher order effect [21].

The diagonalization of the Hamiltonian $H_{\mathrm{e-LO}}$ can also be performed numerically [48]. The results of the exact numerical diagonalization confirm the picture found by the Davydov method and account also for the second-order resonance.

3.2 Excitonic polaron

The exciton states are found by diagonalizing the Hamiltonian

$$H_{\mathrm{X}} = H_{\mathrm{e}} + H_{\mathrm{h}} + H_{\mathrm{C}}, \tag{15}$$

where the components are given by equations (1, 3). We restrict ourselves to the case of a cylindrically symmetric dot ($\lambda = 0$).

The exciton energies for a quantum dot with $\hbar\omega_{0,\mathrm{e}} = 60$ meV for $B = 0$ are shown in Figure 2. For a cylindrical dot, the total orbital momentum M of the interacting carrier pair is a good quantum number which is used to label the levels; within one value of M the levels are numbered by another quantum number $n = 0, 1, ...$ The dominant contribution to the lowest excited states of the exciton comes from the excited hole states, while the electron wavefunction is only slightly modified (Fig. 3). Therefore, the shell structure, originating from the degeneracy of the hole Fock–Darwin levels, is clearly visible in the lower part of the spectrum: the non-degenerate $S = 0$ shell consists of the $M = 0$, $n = 0$ state, the doubly-degenerate $S = 1$ shell is formed by the $M = \pm 1$, $n = 0$ states, and so on, all the levels with $2n + |M| = S$ form

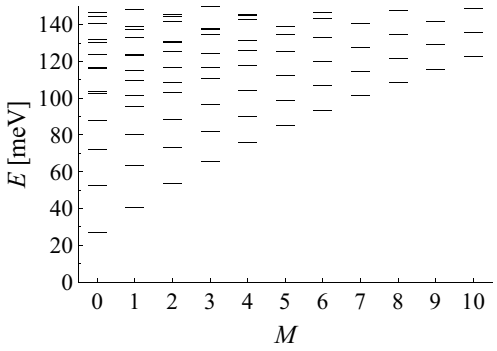

Fig. 2. The spectrum of the exciton in the quantum dot at $B = 0$.

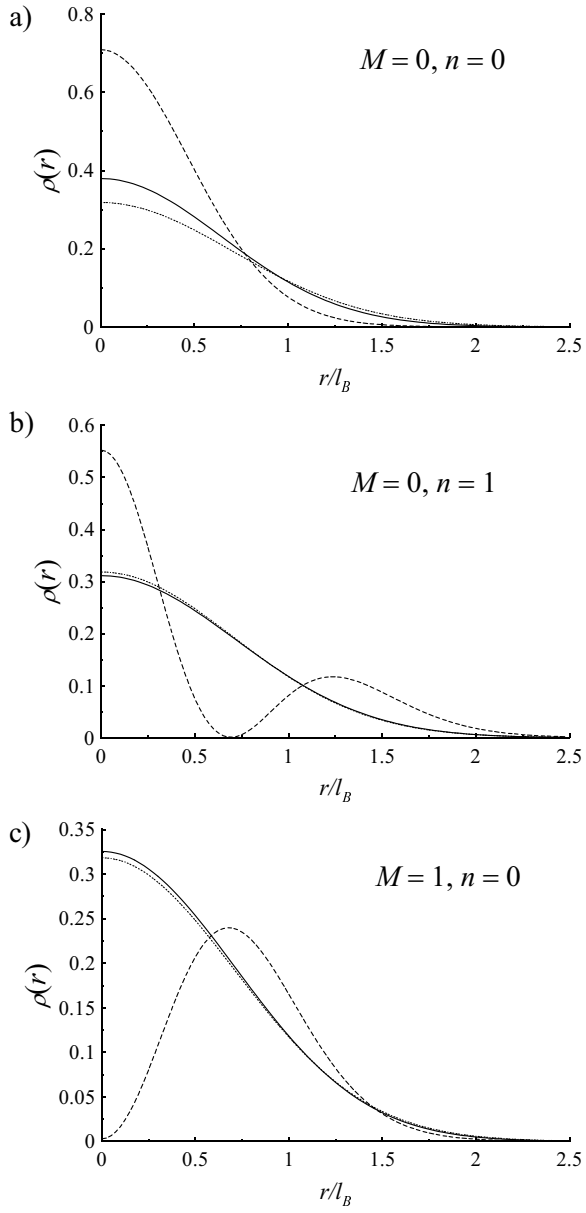

Fig. 3. Electron (solid lines) and hole (dashed lines) probability densities compared to the ground state probability density for a noninteracting particle (dotted lines).

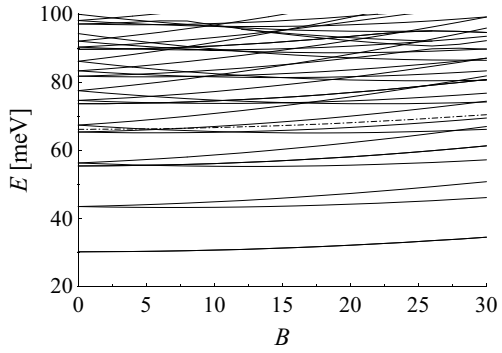

Fig. 4. Exciton spectrum in magnetic field. Dashed line shows the energy $\epsilon_0 + \hbar\Omega$, crossing the $S = 3$ shell.

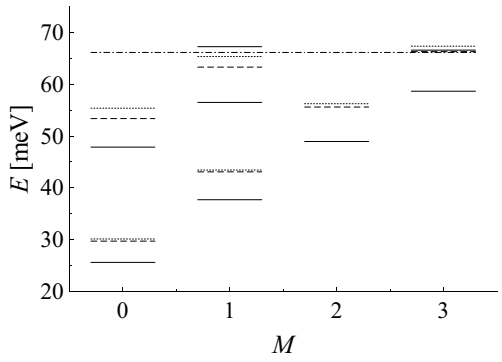

Fig. 5. The excitonic polaron levels at $B = 0$ (solid lines) and the bare exciton levels (dotted lines). For comparison, the results of the adiabatic (independent-boson) calculations are shown (dashed lines). The levels are grouped by the angular momentum M.

the shell S with $(S+1)$–fold degeneracy. This exciton shell structure appears also for more realistic modeling of the dot confinement [43] and is known to modify the optical spectra [51]. However, unlike in the single carrier case, the shells are not equidistant due to the decreasing Coulomb energy gain: the energy separation decreases, like in the atomic shell structure.

The evolution of the lowest levels with growing magnetic field is shown in Figure 4. The degeneracy of the levels with $M \neq 0$ is lifted and the shells become split according to the angular momentum of each state, but for weak fields the shell structure of the lowest shells is still preserved and the levels remain closely grouped. The relatively slow evolution of the lowest exciton levels, formed mostly by exciting the hole, is due to the large hole mass.

The exciton wavefunctions resulting from the numerical diagonalization may be decomposed in the form

$$\Psi_\nu(\mathbf{r}_\mathrm{e}, \mathbf{r}_\mathrm{h}) = \sum_\nu c^\nu_{nm} \Psi_n(\mathbf{r}_\mathrm{e}) \Psi_m(\mathbf{r}_\mathrm{h}), \tag{16}$$

where $\Psi_n(\mathbf{r})$ are the wavefunctions of the noninteracting particles (which have the same form for electrons and holes, as discussed above) and the short-hand symbols n, m, ν comprise the whole set of relevant quantum numbers.

The carrier–LO phonon Hamiltonian,

$$H_{\mathrm{X-LO}} = H_\mathrm{X} + H_\mathrm{F}^{(\mathrm{e})} + H_\mathrm{F}^{(\mathrm{h})} + H_\mathrm{LO}$$

(Eqs. (15, 5) and the LO part of Eq. (4)), may be written in the basis of the excitonic states (16) as

$$H_{\mathrm{X-LO}} = \sum_\nu \epsilon_\nu a^\dagger_\nu a_\nu + \hbar\Omega \sum_{\mathbf{k}} b^\dagger_{\mathrm{o},\mathbf{k}} b_{\mathrm{o},\mathbf{k}} + \frac{1}{\sqrt{N}} \sum_{\nu\nu'\mathbf{k}} F^{\mathrm{X-LO}}_{\nu\nu'}(\mathbf{k}) a^\dagger_\nu a_{\nu'} (b_{\mathrm{o},\mathbf{k}} + b^\dagger_{\mathrm{o},-\mathbf{k}}), \tag{17}$$

where $a^\dagger_\nu, a_\nu$ are the excitonic creation and annihilation operators. The exciton–LO phonon coupling function is

$$F^{\mathrm{X-LO}}_{\nu\nu'}(\mathbf{k}) = F^{\mathrm{e-LO}}_{\nu\nu'}(\mathbf{k}) + F^{\mathrm{h-LO}}_{\nu\nu'}(\mathbf{k}) \tag{18}$$
$$= -\frac{e}{k}\sqrt{\frac{\hbar\Omega}{2v\epsilon_0\tilde{\epsilon}}} \sum_{mnl} \left[c^{\nu *}_{mn} c^{\nu'}_{ln} \mathcal{F}_{ml}(\mathbf{k}) - c^{\nu *}_{mn} c^{\nu'}_{ml} \mathcal{F}_{nl}(\mathbf{k}) \right],$$

where the form-factors $\mathcal{F}_{nn'}(\mathbf{k})$ are given by equation (10).

The Hamiltonian (17) is formally identical to that of a single electron (8) and may be diagonalized by the Davydov method, leading to the diagonal form in terms of the polaronic and modified phononic operators $\alpha_\nu, \alpha^\dagger_\nu$ and $\beta_{\mathrm{o},\mathbf{k}}, \beta^\dagger_{\mathrm{o},\mathbf{k}}$,

$$H_{\mathrm{X-LO}} = \sum_\nu E_\nu \alpha^\dagger_\nu \alpha_\nu + \hbar\Omega \sum_{\mathbf{k}} \beta^\dagger_{\mathrm{o},\mathbf{k}} \beta_{\mathrm{o},\mathbf{k}}. \tag{19}$$

The polaron energy levels E_ν at $B = 0$ are shown in Figure 5. In the description of the carrier–phonon interaction it is often assumed that the non-diagonal coupling terms, $F_{\nu\nu'}(\mathbf{k})$ for $\nu \neq \nu'$, may be neglected. This is equivalent to neglecting the possibility of phonon-induced transitions between the carrier states, *i.e.* to the adiabaticity of the lattice dynamics with respect to the presumably much faster carrier dynamics. The resulting model is known as the independent boson model [24]. Following reference [36] we call this approach *adiabatic approximation*. In order to compare the accuracy of various approaches, in Figure 5 the polaron levels are compared to the bare electron levels and to the values obtained in the adiabatic (independent boson) approximation. As expected, the adiabatic shift for each level is very small due to the charge cancellation. Nevertheless the total shift amounts to a few meV, which is comparable to the energy shift of a confined excess electron [50]. Therefore, it is clear that a quantitatively correct description of polaronic effects for the charge-neutral exciton requires including the coupling to the higher levels, *i.e.* the virtual transitions due to the non-adiabaticity of carrier-phonon interaction.

In the non-resonant case the polaron energy shift (Eq. (13)) is approximated by the usual second-order perturbative correction. Each of the contributions on the right-hand side contains a carrier-phonon interaction matrix element with another state. Comparison between these contributions reveals the accuracy of the independent boson model (only the "diagonal" term) or of any calculation restricted to a certain subset of levels. Figure 6 shows these contributions to the ground level shift

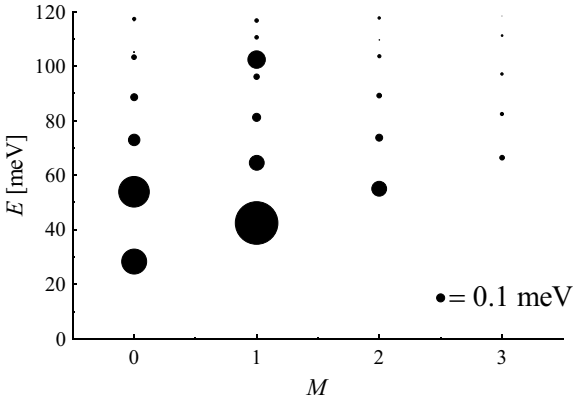

Fig. 6. Contributions to the second order perturbative correction for the ground level energy. The radius of each bubble is proportional to the term involving the matrix element of the carrier-phonon interaction between the ground state and another state, represented by the position of the bubble (*cf.* Fig. 2).

from higher excitonic levels. The large contribution from the excited states is favored not only by orthogonality between the electron and hole wavefunctions (minimizing the charge cancellation effects) but also by the small inter-shell distance (a few times smaller than for a single electron).

An interesting feature that can be noticed in Figure 5 is the resonant energy level splitting for certain levels, analogous to the single-electron case discussed above. In the excitonic case, this effect has been discussed for the first time in reference [38]. For the dot parameters used here, the energy of the $M = 1$, $n = 1$ level exceeds the ground level energy by approximately the LO phonon energy, leading to a split of the upper of the levels. In view of the relatively dense exciton level distribution, the appearance of such anti-crossings in the spectrum of a typical dot should be a rule rather than an exception. An interesting feature, emerging from the grouping of the exciton levels in shells, is the shell nature of the phonon resonances: all the levels in the shell are split.

In view of the slow evolution of the spectrum with magnetic field and the preservation of the shell structure, the resonances found at $B = 0$ can be expected to appear in a wide range of magnetic fields. Figure 7a shows the evolution of the four lowest shells with magnetic field. The shells $S = 0, 1, 2$ are only shifted down, while the shell $S = 3$ is split. To analyze the nature of this split, in Figure 7b we show two levels ($M = +1, +3$) of this resonant shell in a wide range of the magnetic fields. Although the polaron levels are strongly affected by resonances with many low-lying states at strong fields, the general picture is clear. The levels avoid crossing with the energy of the ground state plus one LO phonon, $\epsilon_0 + \hbar\Omega$. The typical anti-crossing structure is exhibited by the $M = 3$ state (dashed line) near $B = -20$ T. The other state ($M = 1$, solid line) evolves in a much more complicated way which is due to the fact that without phonon interaction it is almost parallel to the $\epsilon_0 + \hbar\Omega$ level. Two anti-crossings may

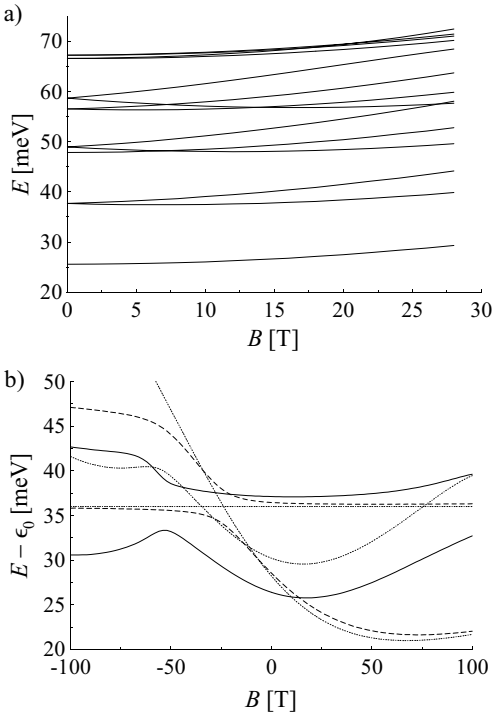

Fig. 7. (a) The spectrum of the excitonic polaron. (b) The structure of the resonant ($S = 3$) shell: the polaronic levels for $M = 1$ (solid line) and $M = 2$ (dashed line) compared to the shifted unperturbed levels (dotted lines).

be traced around $B = -50$ T and around $B = 100$ T. (The bare levels in this figure are shifted to account for the non-resonant interaction with other shells.)

4 Incoherent effects – polaron relaxation

The Davydov transformation allows for a convenient description of the relaxation processes, including the coherent polaronic effects. Although the quantitative estimations will be specified to the single-electron relaxation, the method is general in view of the formal similarity of the Hamiltonians (1) and (17).

The Hamiltonian describing the interaction between the electron and acoustical phonons, equation (6), has the second quantization form

$$H_{\mathrm{DP}}^{\mathrm{e}} = \frac{1}{\sqrt{N}} \sum_{n,n',\mathbf{k}} F_{nn'}^{\mathrm{e-LA}}(\mathbf{k}) a_n^\dagger a_{n'} \left(b_{\mathrm{l},\mathbf{k}} + b_{\mathrm{l},-\mathbf{k}}^\dagger \right), \quad (20)$$

where

$$F_{nn'}^{\mathrm{e-LA}}(\mathbf{k}) = \sigma_{\mathrm{e}} \sqrt{\frac{\hbar k}{2\varrho v c_{\mathrm{l}}}} \mathcal{F}_{nn'}(\mathbf{k}).$$

Together with the Hamiltonian describing the phonon anharmonism (Eq. (7)), this may be written in the polaron

basis as

$$H_{\mathrm{e-ac}} = \frac{1}{\sqrt{N}} \sum_{nn',\mathbf{q}} F^{\mathrm{e-LA}}_{nn'}(\mathbf{q}) \alpha^{\dagger}_{n} \alpha_{n'} (b_{\mathrm{l},\mathbf{q}} + b^{\dagger}_{\mathrm{l},-\mathbf{q}}) + \sum_{\mathbf{k}_1,\mathbf{k}_2,\mathbf{q}} W(\mathbf{k},\mathbf{q}) \beta^{\dagger}_{\mathrm{o},\mathbf{k}} \beta_{\mathrm{o},\mathbf{k}-\mathbf{q}} (b_{\mathrm{t},\mathbf{q}} + b^{\dagger}_{\mathrm{t},-\mathbf{q}}) + \sum_{nn',\mathbf{q},\mathbf{k},s} \tilde{W}^{(s)}_{nn'}(\mathbf{q},\mathbf{k}) \alpha^{\dagger}_{n} \alpha_{n'} \beta_{\mathrm{o},\mathbf{k}} (b_{s,\mathbf{q}} + b^{\dagger}_{s,\mathbf{q}}) + \mathrm{h.c.}, \quad (21)$$

where s runs over the acoustic branches ($s = \mathrm{l}, \mathrm{t}$) and

$$\tilde{W}^{(\mathrm{t})}_{nn'}(\mathbf{q},\mathbf{k}) = -\frac{1}{\sqrt{N}} \frac{F^{\mathrm{e-LO}}_{nn'}(\mathbf{k}+\mathbf{q}) W(\mathbf{k}+\mathbf{q},\mathbf{q})}{E_{n'} - E_n + \hbar\Omega}, \quad (22)$$

$$\tilde{W}^{(\mathrm{l})}_{nn'}(\mathbf{q},\mathbf{k}) = \frac{1}{N} \sum_{n''} \left[\frac{F^{\mathrm{e-LO}}_{n''n'}(\mathbf{k}) F^{\mathrm{e-LA}}_{nn''}(\mathbf{q})}{E_{n'} - E_{n''} + \hbar\Omega} - \frac{F^{\mathrm{e-LO}}_{nn''}(\mathbf{k}) F^{\mathrm{e-LA}}_{n''n'}(\mathbf{q})}{E_{n''} - E_n + \hbar\Omega} \right]. \quad (23)$$

The first term in (21) describes the polaron–LA phonon interaction. Because of the bottleneck effect [29,28] it could lead to real transitions only for energy level distance not exceeding a few meV, which is not the case for a self-assembled dot. The second term describes anharmonic interaction of LO phonons with TA phonons, whereas the last term describes the two-phonon relaxation of the polaron. The LO–TA anharmonism-induced relaxation channel corresponds to equation (22) while the LO–LA channel to equation (23). Both these channels lead to a change of the polaron state accompanied by the creation or annihilation of a pair of phonons: the optical and the acoustical one. At low temperatures only emission process is possible with the probability given by (according to the Fermi golden rule)

$$w^{(s)}_{nn'}(\mathbf{q},\mathbf{k}) = \frac{2\pi}{\hbar} |\tilde{W}^{(s)}(n,n',\mathbf{q},\mathbf{k})|^2 \delta(E_n - E_{n'} - \hbar\Omega - \hbar\omega_s(\mathbf{q})).$$

The relaxation probability is given by the sum

$$w_{n\to n'} = \sum_{\mathbf{k},\mathbf{q},s} w^{(s)}_{nn'}(\mathbf{q},\mathbf{k}).$$

The relaxation probability *via* the two-phonon LO–TA channel may be written as [48,50]

$$w^{(\mathrm{t})}_{n\to n'} = \frac{2}{\pi} \frac{J_{nn'} \gamma^2 q_{\mathrm{t}} v}{\hbar^4 c_{\mathrm{t}}^3}, \quad (24)$$

where $q_{\mathrm{t}} = (E_n - E_{n'} - \hbar\Omega)/\hbar c_{\mathrm{t}}$ (limited by the maximum frequency for TA phonons) and the value of γ may be found by fitting to the experimental data [48,50].

Let us now estimate the polaron relaxation rate from the first excited state to the ground state. The energy conservation restricts this process to a certain energy range over the LO phonon energy, determined by the maximum energy of the TA phonon, ~ 8 meV. Comparing with the diagram of the spectrum (Fig. 1), one sees that the double emission process may take place only for the upper branch of this energy level and only for magnetic fields $B > 25$ T (taking into account the actual LO phonon dispersion restricts this process even further [48]). The polaron relaxation times obtained in this way are even of order of 10 ps (but only in the region of very high magnetic fields).

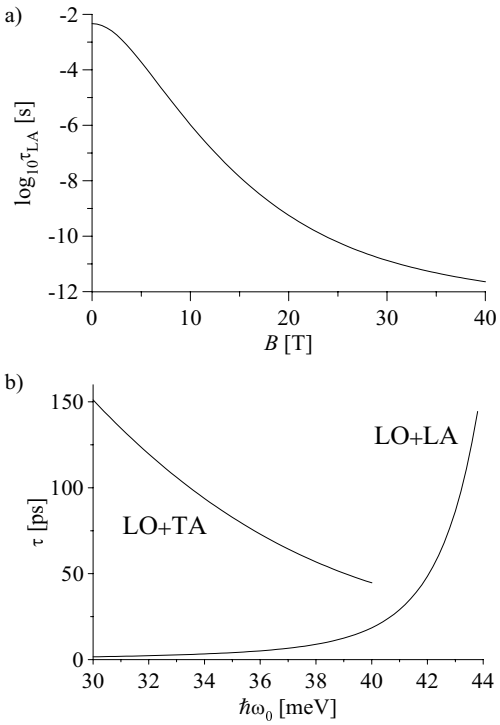

Fig. 8. (a) Magneto–polaron relaxation time from the upper branch of the first excited level with respect to the LO–LA emission ($T = 0$). (b) Relaxation times with respect to the LO–TA anharmonism induced channel and to the LO–LA channel for various dots at $B = 0$. Note that, when the relaxation times from this branch are getting very short, the other polaron branch becomes stable.

The suppression of the relaxation process at low magnetic fields is characteristic of dots with the confinement energy $\hbar\omega_{0,\mathrm{e}}$ exceeding the phonon energy $\hbar\Omega$ by several meV. For larger dots (weaker confinement, $\hbar\omega_{0,\mathrm{e}} <$ 40 meV) the relaxation channel by the LO–TA phonon emission becomes allowed. The corresponding relaxation times are shown in Figure 8b.

Let us note that the anharmonism-induced channel is not subject to the bottleneck effect since it does not involve the direct carrier–LA phonon coupling.

The LO–LA channel may be responsible for polaron relaxation in a wider range of magnetic fields due to the much higher energies of the LA phonons in GaAs (up to 24 meV [47]). The probability of relaxation has the form

[retaining only the largest terms in $\tilde{W}^{(\mathrm{l})}_{nn'}(\mathbf{q},\mathbf{k})$]:

$$w^{(\mathrm{l})}_{n\to n'} = \frac{\sigma^2 J_{nn'}}{4\pi\varrho\hbar^3 c_{\mathrm{l}}^4 q_{\mathrm{l}} l_{\mathrm{B}}^2}\mathcal{J}_{nn'}, \tag{25}$$

where $q_{\mathrm{l}} = (E_n - E_{n'} - \hbar\Omega)/\hbar c_{\mathrm{l}}$ (limited by the upper frequency limit for LA phonons) and

$$\mathcal{J}_{nn'} = l_{\mathrm{B}}^2 \int \mathrm{d}^3\mathbf{q} |\mathcal{F}_{n'n'}(\mathbf{q}) - \mathcal{F}_{nn}(\mathbf{q})|^2 \delta(q - q_{\mathrm{l}}).$$

The polaron relaxation time from the upper branch of the first excited state with respect to the LO–LA channel for various magnetic fields and dot sizes is plotted in Figure 8a. It is clear that for the self-assembled dot discussed here, with $\hbar\omega_{0,\mathrm{e}} \simeq 58$ meV, the initial state is very long-living for any practically attainable magnetic field. This is due to the two-phonon bottleneck mechanism which strongly suppresses the relaxation unless the polaron energy difference approaches the LO phonon energy so that the required LA phonon is a long-wavelength one.

It is essential to note the fundamental difference between the electron and polaron spectrum: in the former case there is only one spectral branch for each state and it crosses the LO phonon energy. On the contrary, in the polaron case only one of the two spectral branches may be close to this resonant energy while the other is distant enough to guarantee more stability (*cf.* Fig. 1). Even at non-zero temperatures, when absorption processes are possible, it is only in the vicinity of the resonance that both branches are affected by the allowed relaxation processes. A rather unexpected effect is also related to the fact that increasing the Fröhlich electron–LO phonon coupling broadens the anti-crossing and thus reduces relaxation rates by strengthening the bottleneck mechanism [48,50].

The efficiency of the bottleneck mechanism at low magnetic fields depends on the dot size: the relaxation time becomes short when the confinement energy is close to the resonance with LO phonons (Fig. 8b).

The above relaxation times have been obtained in the zero temperature limit. Due to high energy of optical phonons, the occupation of LO phonon states may be neglected up to temperatures of order of 100 K. The temperature dependence of the phonon emission processes, entering through acoustical phonon occupation factors, may be qualitatively inferred from the structure of the polaron spectrum and the requirement of energy conservation. As one of the polaron branches is always separated from the LO phonon resonance by the anticrossing half-width of a few meV, the population of the phonon states involved in the process becomes important only at temperatures of a few tens of kelvin. At lower temperatures, the unstable polaron branch may decay faster but the stable one is very slightly affected.

5 Exciton dressing

Any optical experiment or optical control of carrier states in a quantum dot is based on the coupling between the carriers and the electric field of the electromagnetic wave. By using high-power laser pulses this coupling can be made strong, leading to fast excitation of confined excitons. However, this coupling involves pure electronic degrees of freedom, inducing only carrier transitions which must then be followed by lattice relaxation to the potential minimum corresponding to the newly created charge state. A similar effect leads to the well-known Franck-Condon shift in the optical spectra [52]. In the case of the optical exciton creation, the initial lattice configuration corresponds to zero polarization field and zero deformation, while the eigenstate of the interacting system involves some lattice polarization (LO phonon field) and some deformation (LA phonon field). Thus, the process of the lattice relaxation may be viewed as the formation of the phonon dressing around the confined exciton. Relaxing the lattice to the new minimum may be achieved by dissipating the excess energy *e.g.* by phonon–phonon or phonon–carrier scattering. However, as we show below, the energy dissipation may be provided by radiating phonons out of the dot area, for which the phonon dispersion (non-vanishing group velocity) is of major importance, governing the dressing times.

Let us neglect the LO–TA anharmonic interaction and consider the Hamiltonian

$$H = H_{\mathrm{X-LO}} + H_{\mathrm{ac}} + H^{(\mathrm{e})}_{\mathrm{DP}} + H^{(\mathrm{h})}_{\mathrm{DP}}, \tag{26}$$

where the components are given by equations (17, 6) and the LA part of (4). We assume linear LA phonon dispersion and introduce a phenomenological model of the LO phonon dispersion, $\omega_{\mathrm{o}}(\mathbf{k}) = \Omega_0 - \mu k^2$. Fitting to the experimental data [47] yields $\mu \approx 0.06$ meV nm^2, although this estimation might be affected by large uncertainty due to the extremely weak dispersion near $\mathbf{k} = \mathbf{0}$ compared to the experimental accuracy.

The dressing process may be conveniently described using the basis of perturbative eigenstates of the Hamiltonian (26), obtained by the diagonalizing unitary operator e^{S}. (For LO phonons this is the polaronic basis and S is given by (12), neglecting higher order corrections.) After the instantaneous carrier excitation (ultra-non-adiabatic limit), the system is in the bare exciton state. Let us assume, for simplicity, that it is the ground state. To the lowest order, the creation operator for this state may be expressed in the new basis (in the non-resonant case) as

$$\begin{aligned} a_0^\dagger &= \mathrm{e}^{\mathsf{S}}\alpha_0^\dagger \mathrm{e}^{-\mathsf{S}} \\ &= \left(1 - \frac{1}{2N}\sum_{n,s,\mathbf{k}} |\phi^{(s)}_{0n}(\mathbf{k})|^2 (2\beta^\dagger_{s,\mathbf{k}}\beta_{s,\mathbf{k}} + 1)\right)\alpha_0^\dagger \\ &\quad + \frac{1}{\sqrt{N}}\sum_{n,s,\mathbf{k}} \phi^{(s)*}_{0n}(\mathbf{k})\alpha_n^\dagger \left(\beta^\dagger_{s,\mathbf{k}} + \beta_{s,-\mathbf{k}}\right), \end{aligned}$$

where s denotes the phonon branch (LO or LA) and

$$\phi^{(s)}_{0n}(\mathbf{k}) = \frac{F^{(s)}_{0n}(\mathbf{k})}{E_0 - E_n - \hbar\omega_s(\mathbf{k})},$$

where $F_{0n}^{(\mathrm{l})}(\mathbf{k}) \equiv F_{0n}^{(\mathrm{X-LO})}(\mathbf{k})$ is given by (18) and $F_{0n}^{(\mathrm{a})}(\mathbf{k})$ is the corresponding quantity for LA phonons.

The time evolution under the diagonalized Hamiltonian is

$$\alpha_n^\dagger(t) = \alpha_n^\dagger \mathrm{e}^{\mathrm{i}\frac{E_0}{\hbar}t}, \quad \beta_{s,\mathbf{k}}^\dagger(t) = \beta_{s,\mathbf{k}}^\dagger \mathrm{e}^{\mathrm{i}\omega_s(\mathbf{k})t}.$$

Using these formulae, it is easy to write down the exciton retarded Green's function for $t > 0$,

$$\begin{aligned} G_\mathrm{r}(t) &= \langle [a_0(t), a_0^\dagger(0)] \rangle = \langle a_0(t) a_0^\dagger(0) \rangle \qquad (27) \\ &= \left(1 - \frac{1}{N} \sum_{n,s,\mathbf{k}} |\phi_{0n}^{(s)}(\mathbf{k})|^2 (2n_{s,\mathbf{k}} + 1) \right) \mathrm{e}^{\mathrm{i}\frac{E_0}{\hbar}t} \\ &\quad + \frac{1}{N} \sum_{n,s,\mathbf{k}} n_{s,\mathbf{k}} |\phi_{0n}^{(s)}(\mathbf{k})|^2 \mathrm{e}^{-\mathrm{i}(E_n/\hbar - \omega_s(\mathbf{k}))t} \\ &\quad + \frac{1}{N} \sum_{n,s,\mathbf{k}} (n_{s,\mathbf{k}} + 1) |\phi_{n0}^{(s)}(\mathbf{k})|^2 \mathrm{e}^{-\mathrm{i}(E_n/\hbar + \omega_s(\mathbf{k}))t} \end{aligned}$$

where $\langle \cdot \rangle$ denotes the thermal average. The averaging is done only with respect to the phonon states and exciton vacuum [53], hence the equality of the retarded Green's function to the correlation function for $t > 0$. It should be noted that the perturbative treatment is valid only when the above Green's function remains close to one. For a fixed strength of interaction this requires a low enough temperature (in practice, for a typical InAs/GaAs dot, this means $T < 100$ K).

The retarded Green's function is directly related to the system susceptibility in the linear response regime and gives the system response to an instantaneous (δ-shaped) light pulse, generalizing the results of reference [35] to the many-level model. However, it may also be interpreted in terms of the overlap between the initial system state (a bare exciton) and the state after time t, thus describing an inherent system dynamics, independent of the experimental techniques.

In order to explain the time evolution of this function, let us remember that the functions $\phi_{nn'}^{(s)}(\mathbf{k})$ contain the form-factors (10), effectively selecting a certain wavenumber range $k_0^{(s)} \pm \frac{1}{2}\Delta k^{(s)}$, centered around $k_0^{(s)}$ for each branch of phonons ($\Delta k^{(s)} \sim 1/l$, where l is the dot size). This corresponds to a certain frequency range $\omega_0^{(s)} \pm \frac{1}{2}\Delta\omega^{(s)}$, around a central frequency $\omega_0^{(s)}$. The phases that enter in the summation in (27) at the time t spread effectively over the angle range $\omega_0^{(s)}t \pm \frac{1}{2}\Delta\omega^{(s)}t$. When this phase spreading reaches 2π, *i.e.* for $t \sim 2\pi/\Delta\omega^{(s)}$, the last two terms in (27) become small. The asymptotic value of the Green's function is

$$|G_\mathrm{r}(t = +\infty)| = 1 - \frac{1}{N} \sum_{\mathbf{k},n,s} |\phi_{0n}^{(s)}(\mathbf{k})|^2 (2n_{s,\mathbf{k}} + 1).$$

The value of the Green's function may be related directly to the fidelity of an operation performed by the ultrafast pulse on the excitonic states of a single quantum dot (a one-qubit operation for the quantum gate proposal of Ref. [16]). Denoting the reduced density matrix of the qubit by $\varrho_\mathrm{C}(t)$ and the evolution operator for the undisturbed qubit by $U(t)$, and assuming that the initial state is $|0\rangle$ (no exciton), one defines the fidelity as the overlap between the desired final state and the actual state described by $\varrho_\mathrm{C}(t)$,

$$F = 1 - \delta = \langle 0 | U^\dagger(t) \varrho_\mathrm{C}(t) U(t) | 0 \rangle \cdot$$

If the operation is a rotation by the angle α in the two-dimensional space of the qubit, then the fidelity loss δ may be expressed as

$$\delta(t) = \frac{1}{2} \sin^2 2\alpha \left[1 - \mathrm{Re}\Big(G_\mathrm{r}(t) \mathrm{e}^{\mathrm{i}Et} \Big) \right].$$

Hence, the decrease of the Green's function is related to the fidelity loss of the excitonic qubit, *i.e.* it is a measure of decoherence of the qubit state after fast gating.

The decoherence time depends on the phonon dispersion (the frequency range $\Delta\omega^{(s)}$) and weakly changes with temperature. For the acoustical phonons, it is $\tau \sim 2\pi l/c \sim 1$ ps (Fig. 9a). For the nearly dispersionless optical phonons, the dynamics is dominated by slowly vanishing coherent phonon beats (Figs. 9b and 9c). However, this strongly oscillatory dynamics may not be noticeable in a real experiment, where probing the system takes some finite time and the sub-picosecond oscillations are averaged out. Moreover, it is known that the anharmonic LO–TA interaction [44,45] (see Sect. 4, not included in the present description) acts on much shorter timescales and may be expected to considerably shorten this time.

Both for optical and acoustical phonons the time varies with the dot size. In the case of acoustical phonons the position of the final plateau, *i.e.* the asymptotic coherence loss at $t \to \infty$, critically depends on temperature (Fig. 9a).

The long-time coherence of the carrier–LO phonon interaction supports the assumption that the Fröhlich interaction should be treated as a coherent effect [21,50]. It should be remarked that the 100 ps time obtained here is merely a rough estimation, due to the uncertain LO dispersion fitting.

It is possible to see directly that the described process consists in the formation of a coherent (*i.e.* with non-vanishing mean displacement) phonon field corresponding to the classical lattice deformation around the confined charge. Let us consider the mean lattice displacement corresponding to the branch s at the point $\mathbf{r}$ after time t,

$$\begin{aligned} \langle \mathbf{u}_s(\mathbf{r}, t) \rangle = \frac{1}{N} \sum_{\mathbf{k}} \sqrt{\frac{N\hbar}{2\varrho v \omega_s(\mathbf{k})}} \frac{\mathbf{k}}{k} \mathrm{e}^{\mathrm{i}\mathbf{k}\cdot\mathbf{r}} \\ \times \left\langle a_0 \left(b_{s,\mathbf{k}} \mathrm{e}^{-\mathrm{i}\omega_s(\mathbf{k})t} + b_{s,-\mathbf{k}}^\dagger \mathrm{e}^{\mathrm{i}\omega_s(\mathbf{k})t} \right) a_0^\dagger \right\rangle. \end{aligned}$$

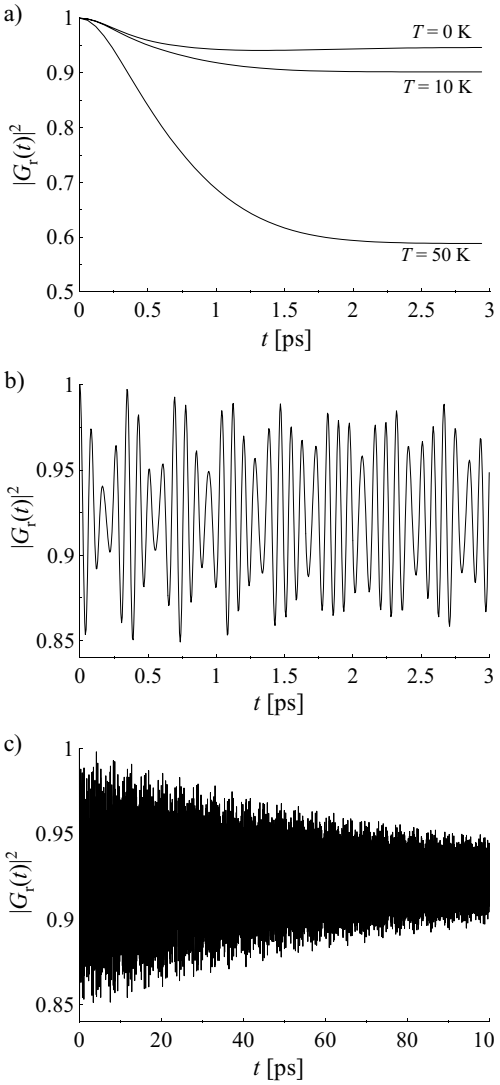

Fig. 9. Dressing-induced decoherence of the exciton due to LA phonons (a) and due to LO phonons: oscillations with LO phonon frequency (b) decay on a very long timescale (c).

Transforming to the diagonalizing basis, as previously, one obtains in the lowest order

$$\langle \mathbf{u}_s(\mathbf{r},t)\rangle = \frac{1}{N}\sum_{\mathbf{k}} \sqrt{\frac{\hbar}{2\varrho v \omega_s(\mathbf{k})}} \times \frac{\mathbf{k}}{k} \mathrm{e}^{\mathrm{i}\mathbf{k}\cdot\mathbf{r}} 2\mathrm{Re}\left[\phi_{00}^{s*}(\mathbf{k})\left(1-\mathrm{e}^{\mathrm{i}\omega_s(\mathbf{k})t}\right)\right].$$

After a sufficiently long time the oscillating term averages to zero (around $\mathbf{r}=\mathbf{0}$) and a time-independent displacement field is formed. Figure 10 shows the mean lattice deformation due to the deformation potential coupling on the dot axis, $\mathbf{r}=(0,0,z)$, at various instances of time. A simple and intuitive picture emerges: formation of the lattice deformation, corresponding to the displaced equilibrium, is accompanied by emitting a phonon packet that carries the excess energy away from the dot with the speed of sound.

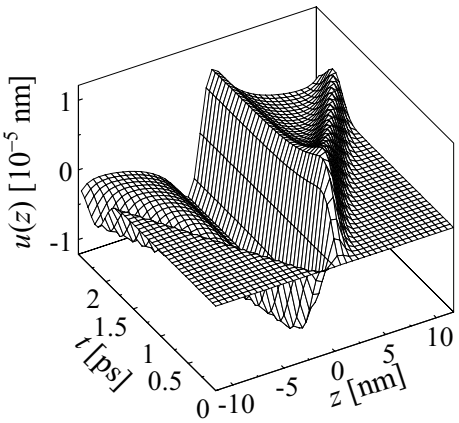

Fig. 10. Time evolution of the mean lattice deformation at the dot axis ($x=y=0$). The time-independent deformation, corresponding to the coherent phonon dressing, is formed around $z=0$ (*i.e.* in the dot area) within ≈ 1 ps. This is accompanied by emission of a phonon packet carrying away the excess energy at the speed of sound, seen on the plot as the ridge and the valley with growing distance from the dot.

6 Conclusions

In this paper we reviewed various manifestations of the carrier–phonon interaction in quantum dots. As compared to the bulk case, the nanometer scale of confinement leads to essentially different phonon phenomena. The energy scale of the confined carriers is close to the resonance with optical phonons, hence the carrier–LO phonon interaction is in the strong coupling regime leading to considerable modification of the carrier spectrum *i.e.* to the polaron effect. The Fröhlich interaction for confined carriers is enhanced by non-adiabatic effects. In contrast to these increased coherent effects, the incoherent carrier–acoustical phonon interaction is diminished due to the large inter-level distance compared to the maximum acoustical phonon energy and to the confinement-related bottleneck effect (size incommensurability). These effects are magnified by wide polaron anti-crossings in the spectrum induced by the increased Fröhlich coupling and lead to the relaxation times of tens of ps (at least one order of magnitude longer than in bulk).

In view of this essential difference with respect to bulk carriers, an alternative analogy may be proposed, where the confined carrier properties are associated with those of an atom. It is clear that, although this "artificial atom" idea may be useful for the description of the basic spectral properties of confined carriers in semiconductors, it may also be strongly misleading. In fact, the analogy with atomic physics is limited by the existence of the upper bound of the phonon spectrum and the much lower speed of sound, as compared to light. As a result, for the energy scales relevant to the "artificial atoms", the importance of short-wavelength phonons grows which leads to the geometrical suppression (bottleneck) effects.

A completely new element in the semiconductor quantum dot physics is the existence of the nearly dispersionless LO phonon branch with the spectrum lying above a

gap comparable to the carrier excitation energies. A boson field of this kind has no analogue in the optical properties of atoms. The interaction with the LO phonons leads to the essential modification of the spectrum: a manifestation of the coherent character of the phenomenon.

The interplay between the coherent and incoherent phonon interaction conforms with the experimental data. The coherent effects related to the LO phonons are responsible for the structure of the spectrum (shifts and anticrossings). The quantitative results agree with the experiment (within the one-phonon approximation). Since the idea of purely LO phonon relaxation contradicts the obviously coherent character of the corresponding channel of interaction, the correct description requires employing mixed processes, involving acoustical phonons. Although these processes are of higher order in the weak carrier–phonon coupling, the relaxation times calculated within this approach agree with the experimental data [30,31]. Large mixing of carrier and phonon states near the LO phonon resonances may be essential for explaning the increase of the observed Huang-Rhys parameter for absorption [33,34] although quantitative comparison is still to be done. Some experimental effects, like the observed coupling to zone edge phonons [30], are clearly outside the range of our model.

Another source of decoherence are lattice relaxation processes following a fast (sub-picosecond) optical carrier excitation in a quantum dot. Due to the slow lattice dynamics, the fast charge excitation must be followed by a relaxation process which may be interpreted as formation of the polarization or deformation dressing around the exciton. Just after the excitation the state of the carrier subsystem does not correspond to a stationary state of the whole interacting system which leads to dephasing on a timescale depending on the effective spectral width of the coupled phonon continuum. For a typical InAs/GaAs dot this decoherence time is of order of a picosecond, while the final degree of the coherence loss strongly depends on temperature and may vary in a wide range. This decoherence scenario is indeed closely related to the "minimal decoherence" idea [54]. This generic effect may be expected in any ultrafast experiment, the recent coherence measurements [19] being an example. The theoretical model [40] closely reproducing the actual experiment confirms this interpretation.

In conclusion, the carrier-phonon interactions in confined semiconductor systems (quantum dots) are manifested by a wide variety of effects, both coherent and incoherent. There is still much to be done to fully understand the physics of these phenomena and to assess their importance for the future technological applications.

Supported by European Commission Project No. IST-1999-11311 (SQID) and KBN Project No. PB 2 PO3B 055 18.

References

1. *The Physics of Quantum Information*, edited by D. Bouwmeester, A. Eckert, A. Zeilinger (Springer, Berlin, 2000)
2. J.I. Cirac, P. Zoller, Phys. Rev. Lett. **74**, 4091 (1995)
3. J. Poyatos, J. Cirac, P. Zoller, Phys. Rev. Lett. **81**, 1322 (1998)
4. L.-M. Duan, J. Cirac, P. Zoller, Science **292**, 1695 (2001)
5. C. Monroe, D.M. Meekhof, B.E. King, W.M. Itano, D.J. Wineland, Phys. Rev. Lett. **75**, 4714 (1995)
6. L. Jacak, P. Hawrylak, A. Wójs, *Quantum Dots* (Springer, Berlin, 1998)
7. C. Pryor, Phys. Rev. B **57**, 7190 (1998)
8. M. Fricke, A. Lorke, J. Kotthaus, G. Medeiros-Ribeiro, P. Petroff, Europhys. Lett. **36**, 197 (1996)
9. M. Kastner, Phys. Today **1**, 24 (1993)
10. R. Ashoori, Nature **379**, 413 (1996)
11. T. Stievater, X. Li, D. Steel, D. Gammon, D. Katzer, D. Park, C. Piermarocchi, L. Sham, Phys. Rev. Lett. **87**, 133603 (2001)
12. H. Kamada, H. Gotoh, J. Temmyo, T. Takagahara, H. Ando, Phys. Rev. Lett. **87**, 246401 (2001)
13. H. Htoon, T. Takagahara, D. Kulik, O. Baklenov, A.L. Holmes Jr, C. Shih, Phys. Rev. Lett. **88**, 087401 (2002)
14. A. Zrenner, E. Beham, S. Stuffer, F. Findeis, M. Bichler, G. Abstreiter, Nature **418**, 612 (2002)
15. D. Loss, D.P. DiVincenzo, Phys. Rev. A **57**, 120 (1998)
16. E. Biolatti, R. Iotti, P. Zanardi, F. Rossi, Phys. Rev. Lett. **85**, 5647 (2000)
17. E. Pazy, E. Biolatti, T. Calarco, I. D'Amico, P. Zanardi, F. Rossi, P. Zoller, *Spin-based optical quantum gates via pauli blocking in semiconductor quantum dots*, `cond-mat/0109337` (2001)
18. M. Bayer, P. Hawrylak, K. Hinzer, S. Fafard, M. Korkusinski, Z. Wasilewski, O. Stern, A. Forchel, Science **291**, 451 (2001)
19. P. Borri, W. Langbein, S. Schneider, U. Woggon, R. Sellin, D. Ouyang, D. Bimberg, Phys. Rev. Lett. **87**, 157401 (2001)
20. N. Bonadeo, J. Erland, D. Gammon, D.S. Katzer, D. Park, D.G. Steel, Science **282**, 1473 (1998)
21. S. Hameau, Y. Guldner, O. Verzelen, R. Ferreira, G. Bastard, Phys. Rev. Lett. **83**, 4152 (1999)
22. P. Fry, I. Itskevich, D. Mowbray, M. Skolnick, J. Finley, J. Baker, E. O'Reilly, L. Wilson, I. Larkin, P. Maksym, M. Hopkinson, M. Al-Khafaji, J. David, A. Cullis, G. Hill, J. Clark, Phys. Rev. Lett. **84**, 733 (2000)
23. M. Korkusinski, P. Hawrylak, Phys. Rev. B **63**, 195311 (2001)
24. G.D. Mahan, *Many-Particle Physics* (Kluwer, New York, 2000)
25. U. Hohenester, R. Di Felice, E. Molinari, Appl. Phys. Lett. **75**, 3449 (1999)
26. U. Hohenester, R. Di Felice, E. Molinari, F. Rossi, Physica E **7**, 934 (2000)
27. S. De Rinaldis, I. D'Amico, E. Biolatti, R. Rinaldi, R. Cingolani, F. Rossi, Phys. Rev. B **65**, 081309 (2002)
28. H. Benisty, C. Sotomayor-Torres, C. Weisbuch, Phys. Rev. B **44**, 10945 (1991)
29. U. Bockelmann, G. Bastard, Phys. Rev. B **42**, 8947 (1990)
30. I.V. Ignatiev, I.E. Kozin, V.G. Davydov, S.V. Nair, J.-S. Lee, H.-W. Ren, S. Sugou, Y. Masumoto, Phys. Rev. B **63**, 075316 (2001)
31. R. Heitz, M. Veit, N. Ledentsov, A. Hoffmann, D. Bimberg, P. Kopaev, Z. Alferov, Phys. Rev. B **56**, 10435 (1997)
32. R. Heitz, I. Mukhametzhanov, O. Stier, A. Madhukar, D. Bimberg, Phys. Rev. Lett. **83**, 4654 (1999)

33. R. Heitz, I. Mukhametzhanov, O. Stier, A. Madhukar, D. Bimberg, Physica E **7**, 398 (2000)
34. A. Lemaître, A. Ashmore, J. Finley, D. Mowbray, M. Skolnick, M. Hopkinson, T. Krauss, Phys. Rev. B **63**, 161309 (2001)
35. B. Krummheuer, V. Axt, T. Kuhn, Phys. Rev. B **65**, 195313 (2002)
36. V. Fomin, V. Gladin, J. Devrese, E. Pokatilov, S. Balaban, S. Klimin, Phys. Rev. B **57**, 2415 (1998)
37. S. Hameau, J. Isaia, Y. Guldner, E. Deleporte, O. Verzelen, R. Ferreira, G. Bastard, J. Zeman, J. Gérard, Phys. Rev. B **65**, 085316 (2002)
38. O. Verzelen, R. Ferreira, G. Bastard, Phys. Rev. Lett. **88**, 146803 (2002)
39. O. Verzelen, S. Hameau, Y. Guldner, J.M. Gérard, R. Ferreira, G. Bastard, Jpn J. Appl. Phys. **40**, 1941 (2001)
40. A. Vagov, V. Axt, T. Kuhn, Phys. Rev. B **65**, 195313 (2002)
41. M.H. Degani, G.A. Farias, Phys. Rev. B **42**, 11950 (1990)
42. A.V. Uskov, A.-P. Jauho, B. Tromborg, J. Mork, R. Lang, Phys. Rev. Lett. **85**, 1516 (2000)
43. A. Wójs, P. Hawrylak, S. Fafard, L. Jacak, Phys. Rev. B **54**, 5604 (1996)
44. F. Vallée, F. Bogani, Phys. Rev. B **43**, 12049 (1991)
45. F. Vallée, Phys. Rev. B **49**, 2460 (1994)
46. S. Adachi, J. Appl. Phys. **58**, R1 (1985)
47. D. Strauch, B. Dorner, J. Phys: Cond. Matt. **2**, 1457 (1990)
48. L. Jacak, J. Krasnyj, D. Jacak, P. Machnikowski, Phys. Rev. B **67**, 035303 (2003)
49. A. Davydov, G. Pestryakov, Phys. Stat. Sol. (b) **49**, 505 (1972)
50. L. Jacak, J. Krasnyj, D. Jacak, P. Machnikowski, Phys. Rev. B **65**, 113305 (2002)
51. P. Hawrylak, G. Narvaez, M. Bayer, A. Forchel, Phys. Rev. Lett. **85**, 389 (2001)
52. G. Mahan, Phys. Rev. B **15**, 4587 (1977)
53. A. Suna, Phys. Rep. **135**, A111 (1964)
54. R. Alicki, M. Horodecki, P. Horodecki, R. Horodecki, Phys. Rev. A **65**, 062101 (2002)